scientific data

OPEN

DATA DESCRIPTOR

A comprehensive dataset of germinoma on MRI/CT with clinical and radiomic data

Lixuan Huang[1,5], Jiangnian Gong[1,5], Daqin Feng[4,5], Ling Zhang[1], Hao Ren[2], Xin Zhao[3], Chang Liu[4], Hui Liang[4], Panlin Mo[4], Minhai Dong[4], Yongjia Yu[4] ✉, Zisan Zeng[1] ✉ & Lun Liang[4] ✉

Intracranial germ cell tumors (GCTs) are rare neoplasms with a peak incidence in adolescents. Germinoma is the most common histological subtype of intracranial GCTs. Its symptoms include intracranial hypertension, visual field defects, and hormonal disorders, affecting the physical health of adolescents. Germinoma is sensitive to chemo-radiotherapy, and most patients do not require neurosurgical resection. Therefore, improving the accuracy of germinoma diagnosis helps to avoid unnecessary surgery. At present, the application of artificial intelligence (AI) in medical imaging has improved the accuracy of disease diagnosis. However, few studies focused on the AI model to diagnosis germinoma and there are no publicly available imaging datasets for germinoma. This study aimed to create a comprehensive dataset for germinoma using magnetic resonance imaging/computed tomography findings with clinical and radiomic data to train and validate AI models. Featuring 65 pathologically confirmed germinomas, the dataset included axial T2-weighted imaging, T2-weighted fluid-attenuated inversion recovery, T1-weighted imaging, T1-weighted imaging with contrast enhancement, diffusion-weighted MR imaging, CT images, clinical data, and morphological and radiomic-based features obtained by segmentation.

Background & Summary

Intracranial germ cell tumors (GCTs) are rare and heterogeneous primary brain tumors that account for 2%–10% of pediatric brain tumors[1–3]. Additionally, the incidence of intracranial GCTs peaks in adolescence (10–19 years old)[4], and their symptoms include intracranial hypertension[5,6], visual field defects, and hormonal disorders[7–9], which seriously affect the physical health and development of adolescents.

WHO classifies GCTs as germinoma and non-germinoma. Germinomas account for 60%–70% of all intracranial GCTs[10]. Although germinoma is a malignant tumor, it is extremely sensitive to chemo-radiotherapy (CRT), and a clinical cure can be achieved with a 5-year survival rate exceeding 90% with radiotherapy alone[11–14]. Therefore, accurate diagnosis is closely related to the treatment and prognosis of patients with germinoma. Clinically, guidelines indicate that neurosurgical resection is necessary for most central nervous system tumors to relieve intracranial hypertension and identify the pathology[15]. However, as CRT is effective against germinoma, patients with germinoma rarely undergo neurosurgical resection unless a residual tumor is present after CRT[16,17]. Moreover, guidelines strongly recommend against aggressive resection of germinoma[18]. To avoid unnecessary neurosurgical resection or biopsy, it is extremely important to improve the accuracy of germinoma diagnosis.

The diagnosis of germinoma depends on imaging, serum/cerebrospinal fluid biomarkers (human chorionic gonadotropin [HCG], HCG β-subunit [β-HCG], α-fetoprotein [AFP]), and pathology using surgical biopsy or resection specimens[18]. Although the combination of routine medical imaging features and biomarkers facilitates the diagnosis of most germinomas, the differential diagnosis of germinoma is limited, and some misdiagnoses occur[19].

[1]Department of Radiology, The First Affiliated Hospital of Guangxi Medical University, Nanning, Guangxi Province, 530021, China. [2]Department of Radiology, The Second Affiliated Hospital of Guangxi Medical University, Nanning, Guangxi Province, 530007, China. [3]Department of Radiology, The Guangxi Medical University Cancer Hospital, Nanning, Guangxi Province, 530021, China. [4]Department of Neurosurgery, The First Affiliated Hospital of Guangxi Medical University, Nanning, Guangxi Province, 530021, China. [5]These authors contributed equally: Lixuan Huang, Jiangnian Gong, Daqin Feng. ✉e-mail: yyjiafish@126.com; zengzisan@aliyun.com; lianglun@sr.gxmu.edu.cn

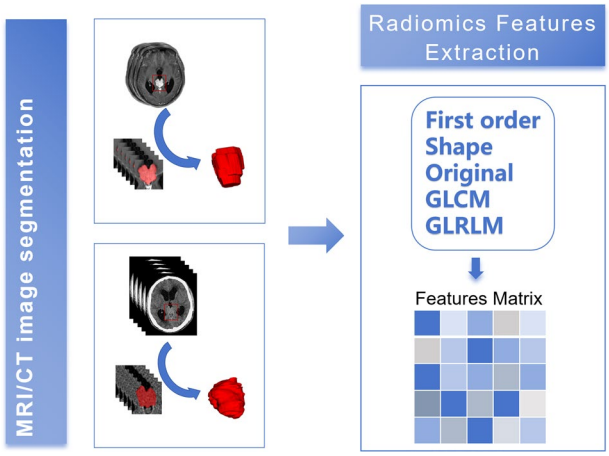

Fig. 1 Flowchart of the construction of a public database of germinoma based on MRI/CT radiomic data.

At present, artificial intelligence (AI), including machine learning (ML) and deep learning algorithms, is increasingly used in disease diagnosis. The application of AI in medical imaging has improved the accuracy of disease diagnosis, reducing laboratory examinations and traumatic pathology[20,21]. Previous studies applied ML algorithms to magnetic resonance imaging (MRI) or texture analysis data to distinguish germinoma from other malignancies[22–25], and the role of AI approaches was affirmed. However, these models were trained and developed using small single-institution hospital datasets that lack diversity regarding patient populations and imaging protocols, which can vary in clinical settings. In fact, AI approaches require large datasets for training and validation, and to date, there are no publicly available imaging datasets for germinoma. Thus, there is a critical need for large, diverse, and open-access datasets to better train AI algorithms and challenge AI models to perform accurate assessments on a large breadth of patient cases.

MRI can produce images of the brain without tissue damage or cranial artifacts, providing important discriminative information for clinicians studying brain tumors[26,27]. Additionally, the European Society for Paediatric Oncology recommended MRI as the primary and standard imaging method for evaluating intracranial GCTs[28]. Conversely, the role of computed tomography (CT) in the diagnosis of germinoma has not been fully studied. Therefore, this study aimed to establish a public database of germinoma that includes clinical data and a set of morphological and radiological features obtained via segmentation-based CT/MRI to provide a basis for further AI-based big data research.

In total, 63 CT and 50 MRI datasets from 65 germinomas obtained from two independently operating hospitals on the same campus were reviewed. The imaging modalities included standard MRI sequences (axial T2-weighted imaging [T2WI], T2-weighted fluid-attenuated inversion recovery [FLAIR], T1-weighted imaging [T1WI], T1-weighted imaging with contrast enhancement [T1WI_CE], and diffusion-weighted MR imaging [DWI]) and CT images, with the caveat that two patients had missing DWI sequences. Semi-automatic segmentations of the results of 65 patients with germinoma generated 1688 different features from each imaging sequence,. Our dataset is publicly available on the figshare repository[29] with all tumor segmentations, standard MRI and CT sequences, clinical data, and a set of morphological and radiomic-based features obtained from the segmentations.

Methods

Subject characteristics. The follow-up imaging studies and clinical data for this study were obtained from two independently operating hospitals on the same campus, namely the First Affiliated Hospital of Guangxi Medical University and Guangxi Medical University Cancer Hospital.

In total, the data of 65 patients newly diagnosed with germinoma via biopsy between May 2015 and April 2024 were retrospectively reviewed. The inclusion criteria were as follows: (1) primary germinoma was confirmed by surgical histopathology and immunohistochemical examination; (2) no surgery, radiotherapy, or chemotherapy was performed before CT and MRI; and (3) surgical treatment was performed within 1 month after preoperative CT/MRI examination. Patients were excluded from the present study according to the following criteria: (1) the tumor was too small and indistinct on CT/MRI and (2) poor image quality precluded measurement.

The 65 patients underwent 63 CT and 50 MRI studies. Of those, 113 studies were segmented as described below. The flow of this study is presented in Fig. 1. The CT and MRI images of the head of a 15-year-old male patient with germinoma were showed in Fig. 2.

Clinical data and anonymization. Clinical data were collected for the 65 patients, including age at diagnosis, sex, pathological and immunohistochemical results, serum tumor marker levels, and serum β-human chorionic gonadotropin (β-HCG). The cohort included 46 males and 19 females aged 6–51 years (mean, 17.09 ± 8.116 years). All 65 patients were pathologically confirmed with intracranial germinoma, including seven patients with β-HCG > 50 mIU/mL, five patients with elevated alpha-fetoprotein (AFP) levels, and elevated carbohydrate antigen 19-9 (CA199) levels in one patient.

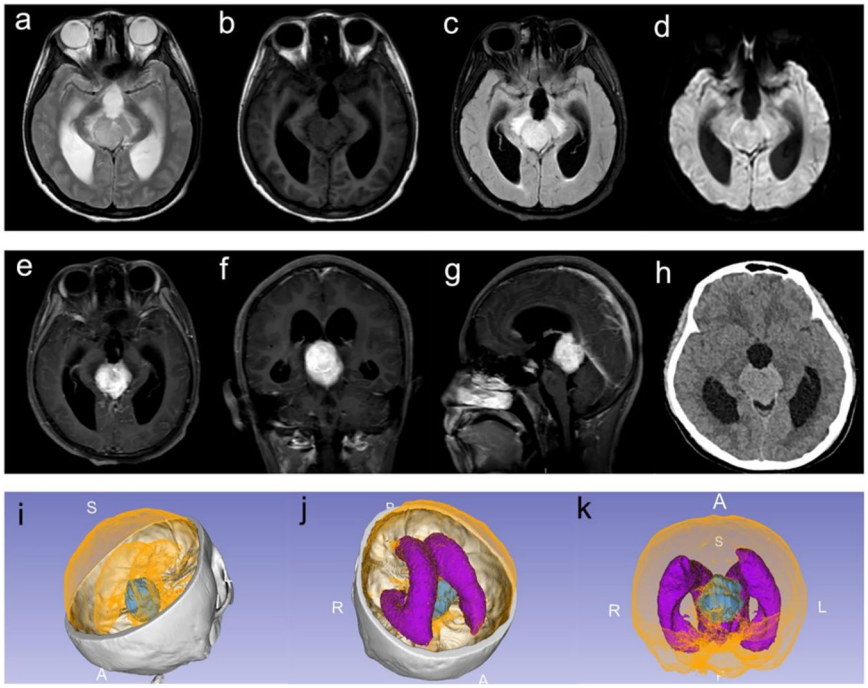

Fig. 2 The CT and MRI images of the head of a 15-year-old male patient who was admitted for 8 days with headache. Head CT scan (h)showed an oval, slightly high-density focus in the pineal region and suprasellar cisterna with clear boundaries, shallow lobed edges and uneven density. MRI showed equal signal on T1WI (**b**), slightly high signal on T2WI (**a**)and FLAIR (**c**), and obvious uniform enhancement on enhanced scan (**e**–**g**). DWI did not show any diffusion-limited signal (**d**). The third ventricle and both lateral ventricles widened. Surgical contraindications were excluded, and pineal tumor resection was performed under general anesthesia. Intraoperatively, the tumor was located in the pineal region, invaded and compressed peripheral blood vessels and brain tissue. The CT-based reconstructions (**i**–**k**) showed the relationship between tumor, brain parenchyma, and ventricular system more clearly, with tumor tissue in blue, brain parenchyma in orange, and ventricular system in purple.

Parameter	T2WI	FLAIR	T1WI	DWI	T1WI_CE
Median (range) Echo time (msec)	80(80–128.6)	120(84–162)	20(2.4–22.7)	79.8(73–102.3)	20(2.4–23.1)
Median (range) Repetition time (msec)	2600(2600-4820)	6000(6000-8002)	2000(149-2161.2)	2404.6(2031.2-7500)	2000(6.4-2940.1)
Median (range) Spacing between slices (mm)	7(6-7.8)	7(6-7.8)	7(6-7.8)	7(6-7.8)	7(4-7.8)
Median (range) Slice Thickness (mm)	6(5-6)	6(5-6)	6(5-6)	6(5-6)	6(3-6)

Table 1. Image parameters from the 50 MRI images segmentations.

Data anonymization was performed using DICOM Anonymizer software (https://www.dicomanonymizer.com). All private Digital Imaging and Communications in Medicine (DICOM) tags and all tags containing the study ID, institution name, institution address, referring physician's name, station name, surgeons' names, manufacturer's model, manufacturer, accession number, study instance ID, and patient name will be replaced. In addition, the patient IDs of CT and MRI of the same patient were randomly replaced with the same string, as was all sensitive or identifying information of segmented images in NIFTI forma for every subject. Furthermore, we utilized the dicom-validator (https://pydicom.github.io/dicom-validator/) to thoroughly verify all our DICOM files, and the results confirmed that these files comply with DICOM standards.

Image acquisition. All T2WI, FLAIR, T1WI, T1WI_CE, and DWI sequences of 50 patients were obtained before treatment. These segmented imaging sequences were acquired using 1.5-T (n = 13) or 3.0-T (n = 37) MRI scanners. Regarding the MRI vendors, General Electric (n = 8), Philips (n = 31), and Siemens (n = 11) medical systems were used. Other image parameters are described in Table 1.

All axial CT plain scan sequences of 63 patients were obtained before treatment. The 65 imaging sequences were acquired with 64-slice(n = 56), 192-slice (n = 5), or 256-slice (n = 2) CT/multi detector-row computed tomography (MDCT) scanners. Regarding the CT imaging vendors, General Electric (n = 13) and Siemens (n = 50) medical systems were used. Other image parameters are described in Table 2.

Parameter	Value	No. of Subjects
Peak kilovoltage (kVp)	130–190	See DICOM image headers for individual scans
X-ray Tube Current (mA)	69–559	See DICOM image headers for individual scans
Slice Thickness (mm)	0.6	1
	0.625	3
	1	46
	1.25	6
	5	7

Table 2. Image parameters from the 63 CT images segmentations.

Segmentation procedure. All MRI and CT images of the enrolled patients were exported from the PACS system in the DICOM format, and we used open-source ITK-SNAP software (www.itksnap.org, version 3.6.0) for semi-automatic segmentation[30–32]. In ITK-snap software, use the Active Contour (aka 'Snake') Segmentation Mode from the Main Toolbar to perform semi-automatic segmentation. Then, select the Threshold mode (upper and lower thresholds) in Segment 3D for manual adjustment, In the T2WI sequence, the ranges for the Lower Threshold and Upper Threshold are 505~728 and 621~1456, respectively. In the FLAIR sequence, they are 253~305 and 378~440, respectively. In the T1WI sequence, they are 91~209 and 218~499, respectively. In the DWI sequence, they are approximately 180~321 and 276~672, respectively. In the T1WI_CE sequence, they are approximately 407~548 and 813~1642, respectively. In the CT plain, they are approximately 25~42 and 84~279, respectively. Segmentations were performed exclusively on the enhancing component of the tumor, as observed on T1-weighted post-contrast images, and do not include other sites of disease in the brain, such as tumor deposits in the lateral ventricles. The segmentations were then checked and manually revised layer by layer as needed by two radiologists with 8 and 10 years of experience, respectively, in brain diagnosis without knowledge of the patients' clinical records. One of the radiologists (with 5 years of experience) performed the second round of segmentation 4 weeks after the initial segmentation. The key points for image segmentation was to avoid tumor bleeding, necrosis, and cystic lesions. The three-dimensional volume (VOI) of interest of the primary tumor on T2WI, FLAIR, T1WI, DWI, T1WI_CE, and CT images were obtained.

Radiomic-based features. The FeAture Explorer Pro (FAE, version 0.5.12, https://sourceforge.net/projects/feature-explorer/) in Python (version 3.7.6)[33] was to extract radiomics features. When extracting the image radiomics features of the images, the images were resampled (1 mm × 1 mm × 1 mm)[34–36], and the intensity of discretization at gray level was set to 16. In total, 1688 different features were extracted for T2WI, FLAIR, T1WI, DWI, T1WI_CE, and CT respectively for each patient. This feature dataset included shape descriptors. The intensity features included simple first-order statistics and those derived from the gray-level co-occurrence matrix (GLCM), gray-level run-length matrix (GLRLM), gray-level size-zone matrix (GLSZM,), neigh-boring gray-tone difference matrix (NGTDM), and gray-level dependence matrix (GLDM).

Ethical approval. This study complied with all relevant ethical regulations. This retrospective research was approved by the ethics committees of the First Affiliated Hospital of Guangxi Medical University (No. 2024-E338-01, 2024) and Guangxi Medical University Cancer Hospital (No. LW2024075,2024). Owing to the retrospective design, the requirement for individual informed consent was waived for this study. The ethics approvals also permitted the open publication of the data.

Data Records

All data records collected in this study can be found in the figshare repository[29]. The original medical images from each follow-up study were stored using digital imaging techniques in the DICOM format. The segmented images of the tumor and the matched original medical images were stored in the NIfTI format after segmentation. We have uploaded a zip file including three files: one file contains the data of all patients in the DICOM format; one file contains the data of all patients in the NIfTI format, all segmented images (file named 1.seg.nii), and the corresponding original images (file named 1.nii); and one file contains seven excel files, including all clinical data and radiomic features (with morphologic features) computed in segments for each subsequent study. All image information was anonymized for each patient.

Technical Validation

Data collection. In total, 65 patients newly diagnosed with germinoma via biopsy were retrospectively reviewed. Only patients in whom germinoma was confirmed by craniotomy of the tumor (n = 60) or ventriculoscopy (n = 5) were included in the study.

Data curation and testing of the inclusion criteria were performed by a neurosurgeon with extensive experience in brain diagnosis and then cross-checked by a different expert.

Segmentation method. All semi-automatic segmentations performed in this study were carefully validated by an expert radiologist after having been performed by experienced experts in the CT or MRI images and cross-checked by another expert.

Consistency analysis. In addition, to evaluate the reproducibility of the extracted feature values, 20 patients were randomly selected for tumor segmentation 1 month later by the same expert radiologist and a second radiologist. They both had no knowledge of the patients' clinical and pathologic details. Subsequently, intraobserver consistency analysis was performed on the images drawn by the same radiologist, and interobserver consistency analysis was performed on the images drawn by both radiologists. An ICC cutoff of >0.75 was utilized to identify stable and reproducible features.

Usage Notes

The entire dataset can be downloaded from the figshare repository[29]. To process the provided images and segmentations, it is highly recommended to use medical imaging tools. We verified that all NIfTI files (segmentations and images) and DICOM files can be loaded correctly with 3D-Slicer (https://www.Slicer.org).

Code availability

No custom code was used.

Received: 24 June 2024; Accepted: 7 February 2025;
Published online: 21 February 2025

References

1. Packer, R. J., Cohen, B. H. & Cooney, K. Intracranial germ cell tumors. *The oncologist* **5**(4), 312–320 (2000).
2. Weiner, H. L. & Finlay, J. L. Surgery in the management of primary intracranial germ cell tumors. *Childs Nerv Syst* **15**, 770–73, https://doi.org/10.1007/s003810050469 (1999).
3. Ogiwara, H. *et al*. Apparent diffusion coefficient of intracranial germ cell tumors. *J Neurooncol* **121**(3), 565–571, https://doi.org/10.1007/s11060-014-1668-y (2015).
4. Goldman, S. *et al*. Phase II Trial Assessing the Ability of Neoadjuvant Chemotherapy With or Without Second-Look Surgery to Eliminate Measurable Disease for Nongerminomatous Germ Cell Tumors: A Children's Oncology Group Study. *J Clin Oncol* **33**(22), 2464–2471, https://doi.org/10.1200/JCO.2014.59.5132 (2015).
5. Takami, H., Graffeo, C. S., Perry, A., Giannini, C. & Daniels, D. J. The Third Eye Sees Double: Cohort Study of Clinical Presentation, Histology, Surgical Approaches, and Ophthalmic Outcomes in Pineal Region Germ Cell Tumors. *World neurosurgery* **150**, e482–e490, https://doi.org/10.1016/j.wneu.2021.03.030 (2021).
6. Hankinson, E. V., Lyons, C. J., Hukin, J. & Cochrane, D. D. Ophthalmological outcomes of patients treated for pineal region tumors. *Journal of neurosurgery. Pediatrics* **17**(5), 558–563, https://doi.org/10.3171/2015.10.PEDS15415 (2016).
7. Takami, H., Graffeo, C. S., Perry, A., Giannini, C. & Daniels, D. J. Epidemiology, natural history, and optimal management of neurohypophyseal germ cell tumors. *Journal of neurosurgery* **134**(2), 437–445, https://doi.org/10.3171/2019.10.JNS191136 (2020).
8. Jorsal, T. & Rørth, M. Intracranial germ cell tumours. A review with special reference to endocrine manifestations. *Acta oncologica* **51**(1), 3–9, https://doi.org/10.3109/0284186X.2011.586000 (2012).
9. Sethi, R. V. *et al*. Delayed diagnosis in children with intracranial germ cell tumors. *The Journal of pediatrics* **163**(5), 1448–1453, https://doi.org/10.1016/j.jpeds.2013.06.024 (2013).
10. Louis, D., Ohgaki, H., Wiestler, O. & Cavenee, W. WHO classification of tumours of the central nervous system (Revised 4th Edition) International Agency for Research on Cancer (IARC): Lyon; 2016.
11. Modak, S. *et al*. Thiotepa-based high-dose chemotherapy with autologous stem-cell rescue in patients with recurrent or progressive CNS germ cell tumors. *J Clin Oncol.* **22**(10), 1934–1943, https://doi.org/10.1200/JCO.2004.11.053 (2004).
12. Souweidane, M. M., Krieger, M. D., Weiner, H. L. & Finlay, J. L. Surgical management of primary central nervous system germ cell tumors: proceedings from the Second International Symposium on Central Nervous System Germ Cell Tumors. *J Neurosurg Pediatr.* **6**(2), 125–130, https://doi.org/10.3171/2010.5.PEDS09112 (2010).
13. Villano *et al*. Descriptive epidemiology of central nervous system germ cell tumors: nonpineal analysis. *Neuro-oncology.* **12**(3), 257–264, https://doi.org/10.1093/neuonc/nop029 (2010).
14. da Silva, N. S. *et al*. Primary chemotherapy for intracranial germ cell tumors: results of the third international CNS germ cell tumor study. *Pediatric blood & cancer.* **54**(3), 377–383, https://doi.org/10.1002/pbc.22381 (2010).
15. Gajjar, A. *et al*. Pediatric Central Nervous System Cancers, Version 2.2023, NCCN Clinical Practice Guidelines in Oncology. *JNCCN.* **20**(12), 1339–1362, https://doi.org/10.6004/jnccn.2022.0062 (2022).
16. Huang, X., Zhang, R., Mao, Y., Zhou, L. F. & Zhang, C. Recent advances in molecular biology and treatment strategies for intracranial germ cell tumors. *WJP.* **12**(3), 275–282, https://doi.org/10.1007/s12519-016-0021-2 (2016).
17. Frappaz, D., Conter, C. F., Szathmari, A., Valsijevic, A. & Mottolese, C. The management of pineal tumors as a model for a multidisciplinary approach in neuro-oncology. *Neuro-Chirurgie.* **61**(2-3), 208–211, https://doi.org/10.1016/j.neuchi.2014.03.003 (2015).
18. Nakamura, H. *et al*. The Japan Society for Neuro-Oncology guideline on the diagnosis and treatment of central nervous system germ cell tumors. *Neuro-oncology* **24**(4), 503–515, https://doi.org/10.1093/neuonc/noab242 (2022).
19. Kanamori *et al*. So-called bifocal tumors with diabetes insipidus and negative tumor markers: are they all germinoma? *Neuro-oncology* **23**(2), 295–303, https://doi.org/10.1093/neuonc/noaa199 (2021).
20. Potočnik, J., Foley, S. & Thomas, E. Current and potential applications of artificial intelligence in medical imaging practice: A narrative review. *Journal of medical imaging and radiation sciences* **54**(2), 376–385, https://doi.org/10.1016/j.jmir.2023.03.033 (2023).
21. Shi, Y. H. & Wang, Q. The Artificial Intelligence-Enabled Medical Imaging: Today and Its Future. *Chin Med Sci J* **34**(2), 71–75, https://doi.org/10.24920/003615 (2019).
22. Chen, B. *et al*. Differentiation between Germinoma and Craniopharyngioma Using Radiomics-Based Machine Learning. *J Pers Med* **12**(1), 45, https://doi.org/10.3390/jpm12010045 (2022).
23. Ye, N., Yang, Q., Liu, P., Chen, Z. & Li, X. A comprehensive machine-learning model applied to MRI to classify germinomas of the pineal region. *Comput Biol Med* **152**, 106366, https://doi.org/10.1016/j.compbiomed.2022.106366 (2023).
24. Fan, Y., Huo, X., Li, X., Wang, L. & Wu, Z. Non-invasive preoperative imaging differential diagnosis of pineal region tumor: A novel developed and validated multiparametric MRI-based clinicoradiomic model. *Radiother Oncol* **167**, 277–284, https://doi.org/10.1016/j.radonc.2022.01.005 (2022).
25. Supbumrung, S., Kaewborisutsakul, A. & Tunthanathip, T. Machine learning-based classification of pineal germinoma from magnetic resonance imaging. *World Neurosurg X* **20**, 100231, https://doi.org/10.1016/j.wnsx.2023.100231 (2023).
26. Villanueva-Meyer, J. E., Mabray, M. C. & Cha, S. Current Clinical Brain Tumor Imaging. *Neurosurgery* **81**(3), 397–415, https://doi.org/10.1093/neuros/nyx103 (2017).
27. Chourmouzi, D., Papadopoulou, E., Marias, K. & Drevelegas, A. Imaging of brain tumors. *Surg Oncol Clin N Am* **23**(4), 629–684, https://doi.org/10.1016/j.soc.2014.07.004 (2014).

28. Morana, G. *et al.* Imaging response assessment for CNS germ cell tumours: consensus recommendations from the European Society for Paediatric Oncology Brain Tumour Group and North American Children's Oncology Group. *The Lancet. Oncology.* **23**(6), e249, https://doi.org/10.1016/S1470-2045(22)00063-8 (2022).
29. Lixuan, H. *et al.* A comprehensive dataset of Germinoma on MRI/CT with clinical and radiomic data. *figshare* https://doi.org/10.6084/m9.figshare.28045148 (2024).
30. Besson, F. L. *et al.* Rapid Contour-based Segmentation for 18F-FDG PET Imaging of Lung Tumors by Using ITK-SNAP: Comparison to Expert-based Segmentation. *Radiology* **288**(1), 277–284, https://doi.org/10.1148/radiol.2018171756 (2018).
31. Yushkevich, P. A. *et al.* User-guided 3D active contour segmentation of anatomical structures: significantly improved efficiency and reliability. *Neuroimage* **31**(3), 1116–1128, https://doi.org/10.1016/j.neuroimage.2006.01.015 (2006).
32. Yushkevich, P. A., Gao, Y. & Gerig, G. ITK-SNAP: An interactive tool for semi-automatic segmentation of multi-modality biomedical images. *Annu Int Conf IEEE Eng Med Biol Soc* **2016**, 3342–3345, https://doi.org/10.1109/EMBC.2016.7591443 (2016).
33. Yang, S. *et al.* FeAture Explorer (FAE): A tool for developing and comparing radiomics models. *PLoS ONE* **8**(15), e0237587, https://doi.org/10.1371/journal.pone.0237587 (2020).
34. Hou, M., Zhou, L. & Sun, J. Deep-learning-based 3D super-resolution MRI radiomics model: superior predictive performance in preoperative T-staging of rectal cancer. *Eur Radiol* **33**(1), 1–10, https://doi.org/10.1007/s00330-022-08952-8 (2023).
35. Han, W. *et al.* Deep Transfer Learning and Radiomics Feature Prediction of Survival of Patients with High-Grade Gliomas. *AJNR Am J Neuroradiol* **41**(1), 40–48, https://doi.org/10.3174/ajnr.A6365 (2020).
36. Park, C. J. *et al.* Radiomics risk score may be a potential imaging biomarker for predicting survival in isocitrate dehydrogenase wild-type lower-grade gliomas. *Eur Radiol.* **30**(12), 6464–6474, https://doi.org/10.1007/s00330-020-07089-w (2020).

Acknowledgements

The study was supported by the First-class discipline innovation-driven talent program of Guangxi Medical University, the National Natural Science Foundation of China (No. 82260554 and No. 82460337), the Natural Science Foundation of Guangxi Province (No. 2023GXNSFBA026092 and No. 2024GXNSFAA010100), the Key Research and Development Program of Guangxi Province (No. 2023AB22116), and the Guangxi medical and health appropriate technology development and application project (No. S2018013). We would like to thank members of the Department of Radiology of the First Affiliated Hospital of Guangxi Medical University and Guangxi Medical University Cancer Hospital for technical support. We thank Medjaden Inc. for scientific editing of this manuscript.

Author contributions

L.H., J.G. and D.F. made substantial contributions to the concept or design of the article, database assembly, tumor segmentation, and clinical data collection for the study, and they drafted the article. L.Z. and C.L. revised the article critically for important intellectual content. H.R. and H.L. revised the article and provided software support. X.Z., M.D. and P.M. performed image transfer and de-identification. Y.Y. and Z.Z. approved the version to be published. L.L. agreed to be accountable for all aspects of the work in ensuring that questions related to the accuracy or integrity of any part of the work are appropriately investigated and resolved.

Competing interests

The authors declare no competing interests.

Additional information

Correspondence and requests for materials should be addressed to Y.Y., Z.Z. or L.L.